ChemPhysMater 3 (2024) 212–219

Contents lists available at ScienceDirect

ChemPhysMater

journal homepage: https://www.keaipublishing.com/en/journals/chemphysmater/

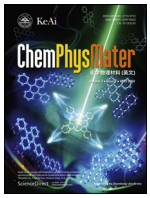

Research Article

Construction of lightweight NiCo-LDH/carbon fiber nanocomposites for broad-band microwave absorption

Shuangshuang Liu, Zhengying Shen, Beibei Zhao, Nannan Wu*

School of Material Science and Engineering, Shandong University of Science and Technology, Qingdao 266590, China

ARTICLE INFO

Keywords:
Microwave absorption
Nickel cobalt layered double hydroxides
Carbon fiber
Interface polarization

ABSTRACT

The rapidly increasing usage of electric technology during the last decades has facilitated the fabrication of high-efficiency microwave absorption (MA) materials (MAMs). In this study, hierarchical NiCo layered double hydroxide (LDH)/carbon fiber (CF) nanocomposites were constructed via simple hydrothermal production, and their MA properties were evaluated. Benefiting from interfacial polarization, defect-induced polarization, and multiple reflections induced by the hierarchical sheets, the LDH/CF composites delivered a better MA performance than that by pure CF and LDH. The addition ratio of the LDH also played a vital role in determining the impedance matching and microwave absorption performance. Specifically, the optimized LDH/CF composites demonstrated an exceptional reflection loss (RL) of −62.47 dB with a thickness of 2.22 mm, and an effective absorption bandwidth (EAB) covering 6.4 GHz (11.6–18.0 GHz) at a 20 wt.% filling ratio, which outperformed the reported CF-based microwave absorbers. Owing to this superior MA, the as-prepared LDH/CF composites demonstrated to be significantly promising for advancing the usage of CF-based MAMs.

1. Introduction

During the last decades, the use of electromagnetic (EM) functional materials is encouraged owing to the rapid advancement of electric gadgets and wireless communication technologies [1,2]. Among the various types of EM functional materials, microwave absorption (MA) materials (MAMs) have gained significant research interest owing to their wide usage in civil and military areas. Numerous investigations have been conducted to construct high-efficiency MAMs with a strong absorbing intensity and thin coating [3]. However, obtaining ideal MAMs with a low density and multi-band absorption is highly challenging.

Carbon fiber (CF) has recently been considered a potential candidate for MA owing to its unique features including a low density and high strength [4]. However, the high conductivity of CF complicates matching the impedance of air [5–8]. Several studies regarding the MA characteristics of CF-based nanocomposites have been conducted owing to the significant influence that impedance-matching has on the MA performance of materials. Liang et al. reported the fabrication of Co_3O_4/carbon cloth (CC) composites as microwave absorbers, for which the strongest reflection loss (RL) reached −46.59 dB and the effective absorption bandwidth (EAB) was 3.04 GHz [9]. The CC@NPC/CoS_2 composites obtained via the in-situ growth of the Co-MOF precursor, calcination, and sulfuration process demonstrated an RL of −59.6 dB at 2.8 mm [10]. These results inferred that rationally decorating CF with semi-conducive constituents can optimize the impedance matching and strengthen the MA [11].

Among the semi-conductive candidates, layered double hydroxides (LDH) are attractive owing to their significantly large specific surface areas, facile synthesis, and distinctive layered structure [12,13]. The combination of LDH with high conductive materials such as MXene and magnetic metals is favorable for improving the MA owing to multiple attenuation mechanisms [11,14–16]. Wang et al. reported the synthesis and MA of a 2D/2D NiFe-LDH/MXene heterostructure, in which LDH served as a moderator to optimize impedance matching. Therefore, the NiFe-LDH/MXene nanocomposites reached an RL_{min} value of −58.2 dB with a 20 wt.% filling ratio [17]. Che demonstrated that the multi-dimensional C@NiCo-LDHs@Ni aerogel with a coating of 2.5 mm delivered an optimal RL value of −57.4 dB and the EAB reached up to 6.4 GHz [18]. Based on the aforementioned articles, the highly conductive CF can be composited with LDHs with a low permittivity to gain a high-efficiency MA.

In this study, NiCo-LDH/CFs were successfully synthesized via a facile solvothermal procedure. The LDH nanosheets were symmetrically deposited on the CF surface and served as platforms to induce interface polarization and multi-reflection. The EM parameters were adjusted by controlling the amount of LDH. The optimal NiCo-LDH/CF sample achieved the strongest *RL* of −62.47 dB at 2.22 mm with a low filler loading of only 20 wt.%. The attenuation mechanisms were thoroughly analyzed.

* Corresponding author.
E-mail address: skd996364@sdust.edu.cn (N. Wu).

https://doi.org/10.1016/j.chphma.2024.01.002
Received 21 November 2023; Received in revised form 27 December 2023; Accepted 7 January 2024
Available online 27 January 2024
2772-5715/© 2024 The Authors. Publishing Services by Elsevier B.V. on behalf of KeAi Communications Co. Ltd. This is an open access article under the CC BY-NC-ND license (http://creativecommons.org/licenses/by-nc-nd/4.0/)

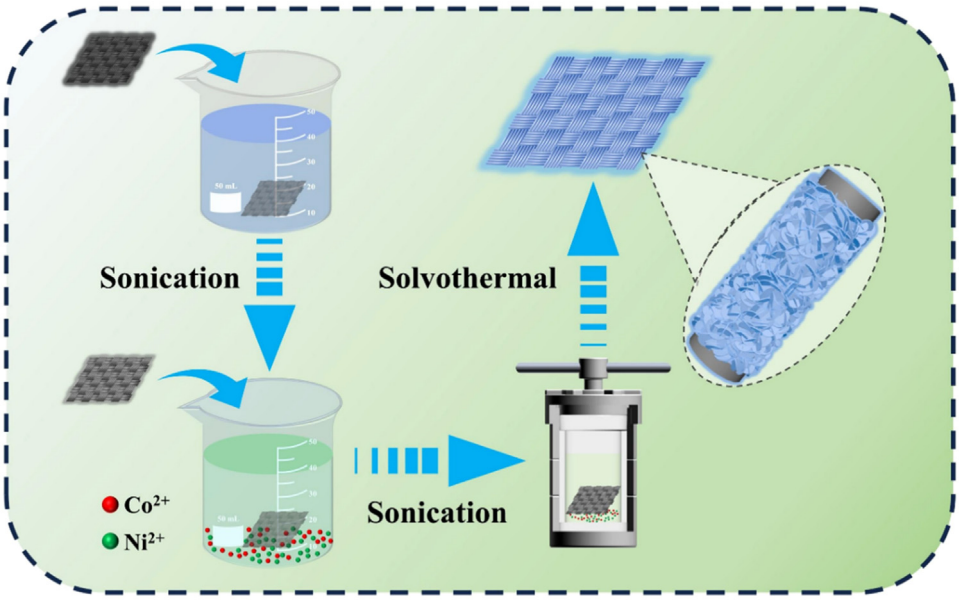

Scheme 1. Synthesis diagram of the NiCo-LDH/CF composites.

2. Experimental

2.1. Materials

Nickel nitrate hexahydrate ($Ni(NO_3)_2{\cdot}6H_2O$) and cobalt nitrate hexahydrate ($Co(NO_3)_2{\cdot}6H_2O$) were obtained from Yongda Chemical Reagent Co., Ltd. and Chengdu Chron Chemicals Co., Ltd., respectively. The urea was purchased from Sinopharm Chemical Reagent Co., Ltd., and the carbon cloth was supplied by Suzhou Sinero Technology Co., Ltd.

2.2. Synthesis of NiCo-LDH/CF composites

As shown in Scheme 1, the CF was successively cleaned with deionized water and ethanol for 15 min. Subsequently, the sonicated CF was immersed in the acid solution for 15 h to improve its hydrophilicity. The NiCo-LDH/CF composite was synthesized using a simple solvothermal method. For the typical synthesis of the NiCo-LDH/CF composites, $Ni(NO_3)_2{\cdot}6H_2O$ (1.5 mM), $Co(NO_3)_2{\cdot}6H_2O$ (0.75 mM), and urea (3 mM) were first dispersed in methanol and sonicated for 30 min. The pretreated CC (2 cm × 2 cm) was then immersed in the mixed solution. The resulting suspension was transferred to an autoclave and sealed, followed by heating at 180 °C for 12 h. The precipitate was recovered by centrifugation after it reached room temperature and was then washed and dried in a vacuum drying oven to obtain the NiCo-LDH/CF composites (Fig. S1). The samples with various additions of $Ni(NO_3)_2{\cdot}6H_2O$ (0, 1.5, and 2.0 mM) and $Co(NO_3)_2{\cdot}6H_2O$ (0, 0.75, and 1.0 mM) were defined as pure CF, CL-1, CL-2.

2.3. Characterizations

The techniques for characterization of the NiCo-LDH/CF are detailed in the Supporting Information.

3. Results and discussions

The X-ray diffraction (XRD) pattern of samples CL-1, CL-2, pure CF, and NiCo-LDH are demonstrated in Fig. 1. Pure CF has two diffraction peaks at 25.5° and 43.8°, which are indexed to the (002) and (101) planes of carbon (PDF No: 41-1487) [19], respectively. The diffraction peaks appearing at 2θ = −11.3°, 22.7°, 33.9°, 38.3°, 44.8°, 59.1°, and

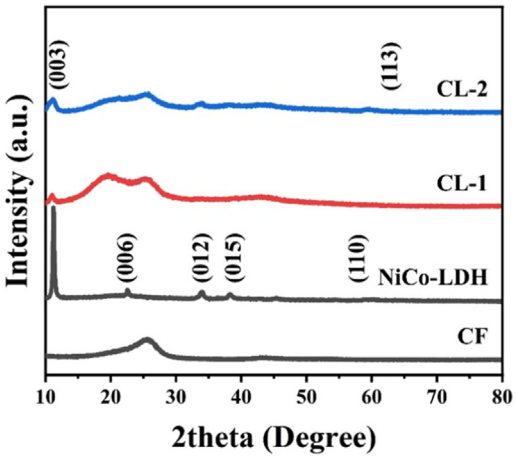

Fig. 1. XRD curves of the CF, NiCo-LDH, and NiCo-LDH/CF.

60.0° correspond to the (003), (006), (012), (015), (018), (110), and (113) planes of the NiCo-LDH (PDF No: 38-0715) [20,21], respectively, which confirms the formation of the NiCo-LDH. At 2θ = 11.3°, CL-2 apparently had a higher diffraction peak intensity compared to CL-1, which is owing to the increased content of Ni^{2+} and Co^{2+}. The curves of samples CL-1 and CL-2 present typical peaks of both the CF (2θ = 25.5°) and LDH (2θ = 11.3°), indicating the successful preparation of the NiCo-LDH/CF composites. The characteristic peaks of (003) and (006) of the NiCo-LDH/CF composites are shifted to the left compared to the pure NiCo-LDH, indicating that the layer spacing of the LDH increased owing to the introduction of anions (NO_3^-) [22].

Pure CFs connected and formed a 3D conductive grid for electron transport, as demonstrated in Figs. 2(a)(b). The NiCo-LDH were composed of abundant nanosheets, as shown in Fig. 2(c). The NiCo-LDH formed by the reaction of Ni^{2+} and Co^{2+} with OH^- under hydrothermal conditions to produce Ni/Co hydroxide, which first formed nanoparticles and subsequently aggregated and crystallized to form multiple nanosheets. Figs. 2(d)–(f) present the images of samples CL-1 and CL-2, demonstrating that attaching the LDH sheets to the surface of CFs results in a hierarchical structure. This structure of multiple nanosheets provides multiple reflective surfaces for the effective attenuation and multi-

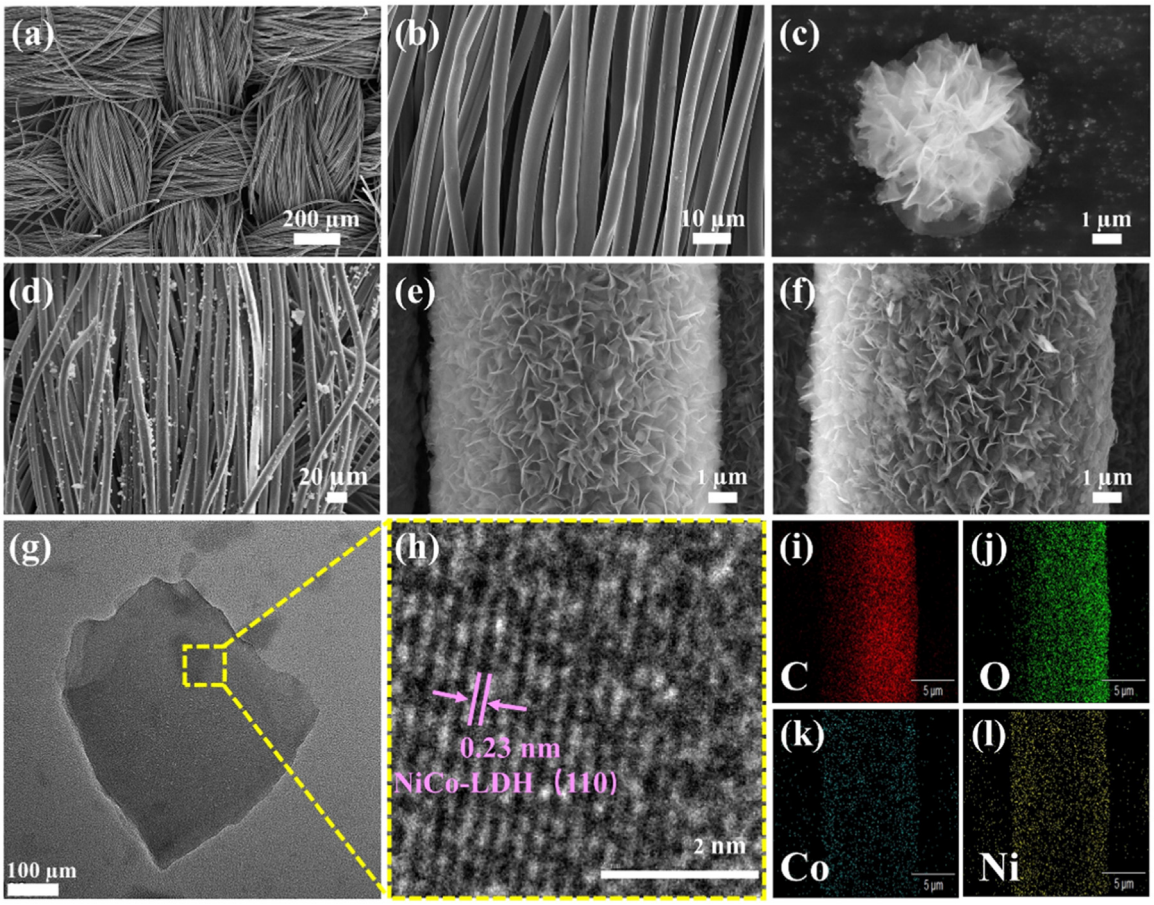

Fig. 2. (a)–(f) SEM images of all the samples. (g)–(h) TEM images of CL-1. (i)–(l) Element mapping of CL-1.

ple scattering of EMW [23]. As the Ni^{2+} and Co^{2+} content increased, the LDH nanosheets became denser, and the diameter of the CF increased. The EDS pattern (Figs. 2(i)–(l)) verified that the NiCo-LDH/CF composites consist of Ni, Co, C, and O, with respective mass percentages of 21.73%, 10.92%, 35.77%, and 31.58%. To further prove the deposition of the NiCo-LDH, characterizations using transmission electron microscopy (TEM) were performed, as shown in Figs. 2(g)(h); the interplanar spacing was 0.23 nm, which fits the (110) plane of the NiCo-LDH [24,25]. Combined with the XRD analysis, NiCo-LDH nanosheets were successfully synthesized.

XPS analysis was conducted to better investigate the chemical bonding state of CL-1, as shown in Fig. 3. The C 1s spectrum appears in Fig. 3(a), along with the typical peaks that are assigned to C–C/C=C (284.09 eV), C–O (284.8 eV), and C=O (287.89 eV), respectively [26–28]. The characteristic peaks of the O 1 s spectrum at 530.95, 532.42, and 533.75 eV can be attributed to the Ni–O/Co–O, vacancy–O, and O adsorbed on the sample surface (Fig. 3(b)) [29]. Two characteristic peaks of Ni $2p_{3/2}$ (855.53 eV) and Ni $2p_{1/2}$ (873.23 eV) may be used to match the Ni 2p spectrum. The satellite peaks are positioned at 861.22 and 878.99 eV (Fig. 3(c)) [21]. Analogously, the peaks at 781.06 and 796.61 eV in the Co 2p spectra are assigned to the Co–O bond, which are the peaks at 785.59 and 802.09 eV that match the satellite peaks [30]. This demonstrates that the primary extant forms of the Co and Ni elements in the NiCo-LDH are Co^{2+} and Ni^{2+}.

To assess the EM absorption performance of the composites, the EM parameters such as the complex permittivity ($\varepsilon_r = \varepsilon' - j\varepsilon''$) and relative complex permeability ($\mu_r = \mu' - j\mu''$) were calculated [31,32]. The real part commonly denotes the power to store the magnetic and electric energies. In contrast, the imaginary part indicates the capability to lose these two types of energies [33–36]. Figs. S2(a) and 4(a)–(c) demonstrate that the ε' values for the sample NiCo-LDH, pure CF, CL-1, and CL-2, varied from 3.2 to 2.8, 16.0 to 7.9, 13.4 to 6.0, and 13.9 to 6.4, respectively, whereas the ε'' ranged from −0.2 to 0.2, 17.0 to 5.0, 6.1 to 2.6, and 6.8 to 2.4. Fig. 4 demonstrates that pure CF possessed the largest permittivity level owing to its high conductivity, whereas the pure LDH demonstrated the lowest permittivity level as a low dielectric component. After decorating the LDH, the permittivity of samples CL-1 and CL-2 ranged between that of CF and LDH. To more clearly illustrate the effect on the EM parameters, the Ni^{2+} and Co^{2+} contents were further increased to 2 and 1 mM, while the amount of CF remained unchanged, and the sample obtained was defined as CL-3. The results in Fig. S3 demonstrate that the ε' and ε'' values possessed a relatively low permittivity level with maximum values of 6.68 and 0.36, respectively, indicating that the addition ratio between the LDH and CF is critical for the EM properties of the composites, and exceeding the decoration of the LDH would be beneficial for the impedance matching of the composites. As shown in Figs. 4(a)–(c), certain apparent peaks were observed for the CL-1 and CL-2 samples, inferring the presence of Debye relaxations. The following is indicated based on the Debye theory (Eqs. (1)(2)) [37–39]:

$$\varepsilon' = \varepsilon_\infty + (\varepsilon_s - \varepsilon_\infty)/(1 + \omega^2\tau^2), \tag{1}$$

$$\varepsilon'' = \varepsilon_p'' + \varepsilon_c'' = (\varepsilon_s - \varepsilon_\infty)\omega\tau/(1 + \omega^2\tau^2) + \sigma/\omega\varepsilon_0. \tag{2}$$

Debye relaxations can be confirmed by drawing Cole-cole semicircles, in which a semicircle represents one polarization relaxation process. As shown in Figs. 5(e)(f), the CL-1 and CL-2 samples exhibited several semicircles, which were mainly derived from dipole polarization and interface polarization. Regarding dipole polarization, the functional groups on the LDH/CF, such as C–O and Ni–O, can act as electric

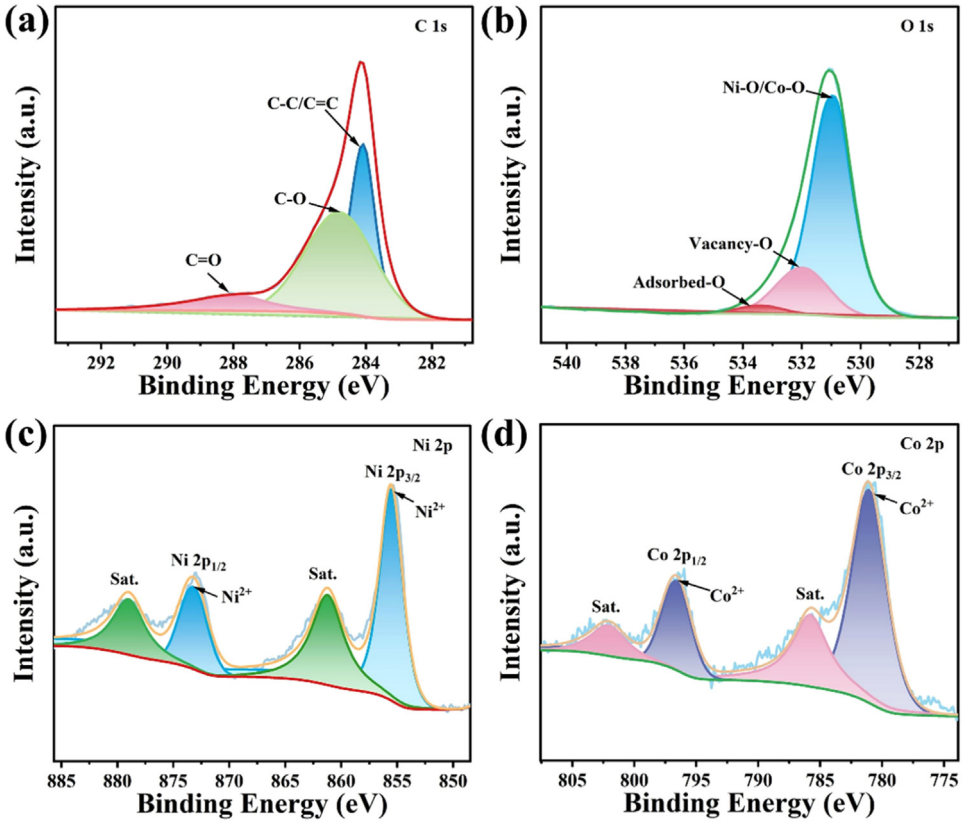

Fig. 3. XPS maps of CL-1: (a) C 1s, (b) O 1s, (c) Ni 2p, and (d) Co 2p.

dipoles and induce dipole polarization owing to the variation of conductivity between the different elements [40,41]. Additionally, the presence of oxygen vacancies (g = 2.005) was further determined by the detection of unpaired electrons using electron paramagnetic resonance (EPR) (Fig. S4), which was compatible with the results of the O 1s spectrum in the XPS. The existence of oxygen vacancies can trap charge carriers and change the distribution of the electron field, thus generating polarization under an alternating EM field, which is also called defect-induced polarization [42,43]. Regarding interface polarization, the positive and negative charges gather at the LDH/CF interface and the redistribution of these charges consumes EM energy. The dielectric and magnetic tangent losses also confirmed the poor magnetic loss ($\tan\delta_\mu = \mu'/\mu''$), and the dielectric loss ($\tan\delta_\varepsilon = \varepsilon'/\varepsilon''$) dominantly contributed to the MA for all the samples shown in Figs. 4(f)(g) [44–47].

The RL values can be calculated based on Eqs. (3)(4) [48,49]:

$$Z_{\text{in}} = Z_0\left(\mu_r/\varepsilon_r\right)^{1/2}\tan h\left\{j\left(2\pi fd/c\right)\left(\mu_r/\varepsilon_r\right)^{1/2}\right\}, \tag{3}$$

$$RL(\text{dB}) = 20\log\left|\left(Z_{\text{in}} - Z_0\right)/\left(Z_{\text{in}} + Z_0\right)\right|. \tag{4}$$

The 3D *RL* curves are displayed in Figs. 5(a)–(c). The CL-1 and CL-2 samples demonstrated an excellent MA performance, as shown in Figs. 5(a)–(c). The RL_{min} values for the pure CF and LDH values were only −10.95 and −3.27 dB, respectively, indicating the weak MA of the CF and LDH (Figs. S2(b)(c)). After modifying the CF with the LDH sheets, the *RL* values of the CL-1 and CL-2 samples reached −62.47 and −55.48 dB, respectively. The corresponding EAB values for the CF, CL-1, and CL-2 samples at various thicknesses were 2.65 GHz at 1.45 mm, 6.4 GHz at 2.22 mm, and 5.44 GHz at 1.72 mm in (Figs. 5(d)–(f)). In particular, the effective absorption for sample CL-2 can be extended to the X and Ku bands by varying the thickness (1.77–2.33 mm) (Fig. 6(b)). The CL-1 and CL-2 samples demonstrated a significantly better MA performance than that of the pure CF and LDH, which can be associated with the degree of impedance matching between the free space and MA. However, as the Ni^{2+} and Co^{2+} content continued to increase, the *RL* of sample CL-3 reached a poor value of −6.0 dB (Fig. S3), which was mainly owing to the excessive addition of LDH making the composite has a relatively low dielectric level. To describe the impedance matching of different samples in a clear pattern, the delta-function method was employed based on Eqs. (5)–(7) [50,51]:

$$K = \frac{\sin\left(\frac{\delta_\varepsilon+\delta_\mu}{2}\right)4\pi\sqrt{\mu'\varepsilon'}}{c\cos\delta_\varepsilon\cos\delta_\mu}, \tag{5}$$

$$M = \frac{4\mu'\cos\delta_\varepsilon\varepsilon'\cos\delta_\mu}{\left(\mu'\cos\delta_\varepsilon - \varepsilon'\cos\delta_\mu\right)^2 + \left[\tan\left(\frac{\delta_\mu-\delta_\varepsilon}{2}\right)\right]\times\left(\mu'\cos\delta_\varepsilon + \varepsilon'\cos\delta_\mu\right)^2}, \tag{6}$$

$$|\Delta| = \left|\sin h^2(Kfd) - M\right|. \tag{7}$$

The more area of with delta values ≤0.4 indicate a better impedance matching condition. Figs. 5(g)–(i) demonstrates that the CL-1 and CL-2 samples covered a larger area ($|\Delta| \le 0.4$) than that of the pure CF sample, which agrees with the MA analysis.

The MA values for the three samples were compared (Fig. 6(a)) considering the absorption intensity, EAB, and matching thickness. All three samples presented a strong absorption intensity, and sample CL-1 possessed the broadest bandwidth. Sample CL-2 demonstrated a broad-band absorption at 1.72 mm, and the EAB could cover a bandwidth ranging from the Ku band to the X band by tuning to 1.77 and 2.34 mm, which is essential for practical applications (Fig. 6(b)). Compared to other carbon-based or LDH composites, the as-fabricated LDH/CF demonstrated a stronger MA and broader EAB (Fig. 6(c)) [52–57].

The results inferred that the LDH/CF can be considered as a superior absorber owing to the optimized impedance matching resulting from the synergy of the LDH and CF, as well as the attenuation mechanisms considering the following aspects (Fig. 7). First, the SEM tests indicated

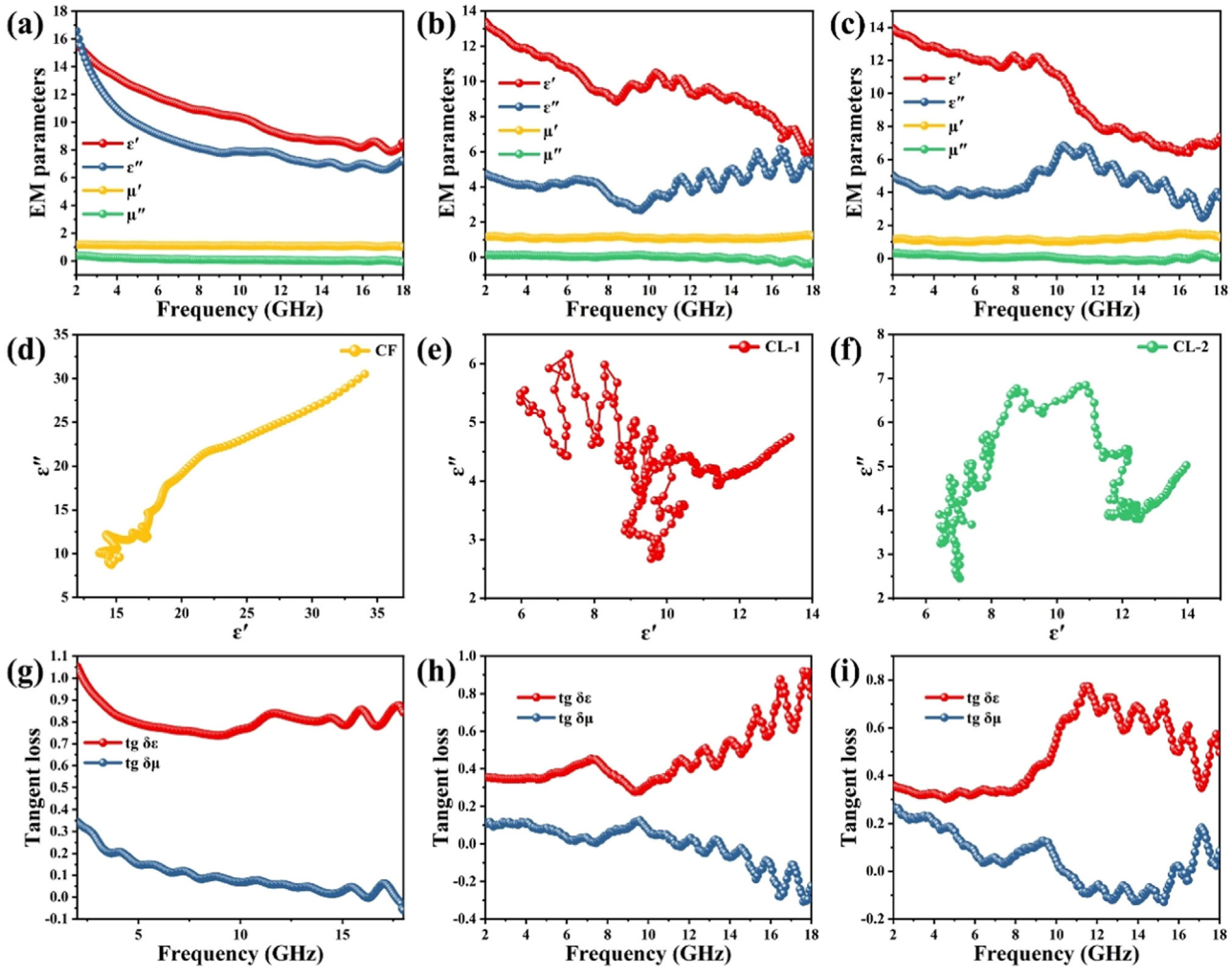

Fig. 4. EM parameters, cole-cole curves, tangent loss of pure CF (a)(d)(g), CL-1 (b)(e)(h), and CL-2 (c)(f)(i).

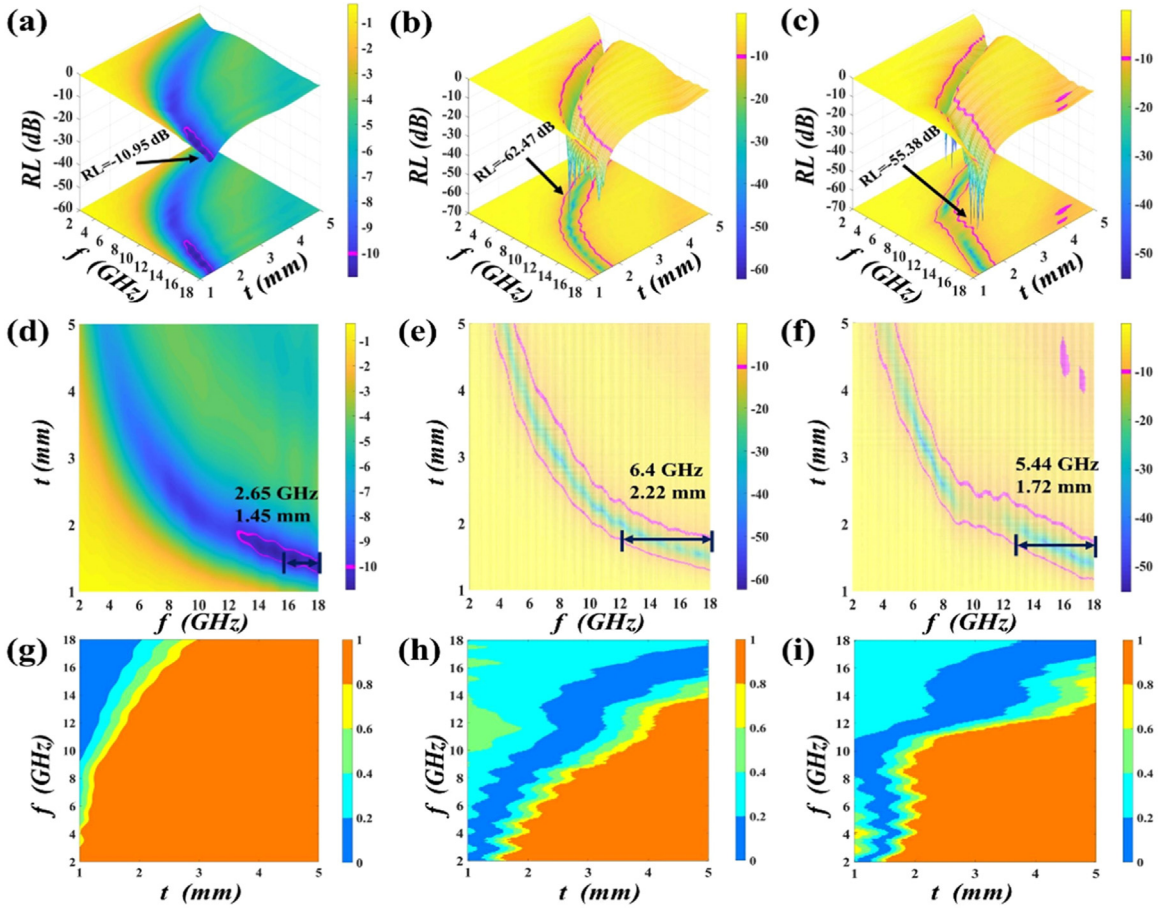

Fig. 5. 3D RL curves, 2D RL curves, and delta value curves of the pure CF (a)(d)(e), CL-1 (b)(e)(f), and CL-2 (c)(f)(i).

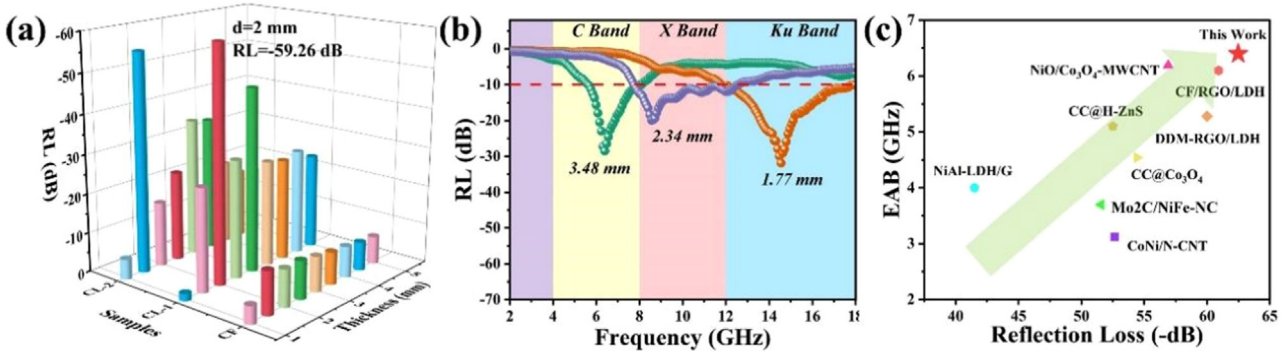

Fig. 6. (a)(b) MA performance of the three samples and CL-2 using different thicknesses. (c) Comparison of the results obtained in this study with various other carbon-based or LDH composites.

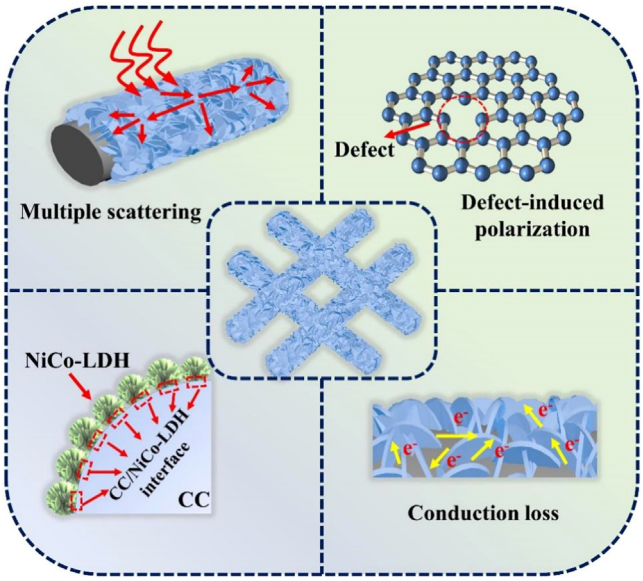

Fig. 7. Schematic illustration of the attenuation mechanisms for the NiCo-LDH/CF.

that the LDH nanosheets were uniformly distributed on the CF surface to form interfaces. The space charges would accumulate at the interfaces between the LDH and CF; when encountering an alternating EM field, these accumulated charges would be forced to redistribute orderly and consume the EM energy during the rearranging process. Second, the EPR tests proved the existence of oxygen vacancies, which would initiate uneven distributions of electric clouds and induce defect-induced polarization. Third, the hierarchical LDH sheets are favorable for creating multiple reflections and the incident EM waves would be consumed from the repeated attenuation. More importantly, based on the measurement of the EM parameters, samples CL-1 and CL-2 possessed a proper dielectric level resulting from the synergy of the LDH and CF for obtaining optimized impedance matching.

4. Conclusions

In summary, NiCo-LDH/CF composites were prepared, in which the abundant LDH sheets were grown on the CF surface to form a hierarchical structure. Modifying the amount of LDH enables optimizing the impedance matching of the CF to an ideal level. The obtained NiCo-LDH/CF composites demonstrated a largely enhanced absorption compared to the pure CF and LDH with the strongest *RL* of −62.47 dB, and the EAB reached a broad value of 6.4 GHz at 2.22 mm. The multiple reflections from hierarchical LDH sheets, defect-induced polarization from oxygen vacancies, and interface polarizations contributed to the attenuation of synergy. Our study provided new methods for developing lightweight CF-based MAMs with a strong MA.

Declaration of Competing Interest

The authors declare that they have no known competing financial interests or personal relationships that could have appeared to influence the work reported in this paper.

CRediT authorship contribution statement

Shuangshuang Liu: Writing – original draft, Validation, Methodology, Investigation, Formal analysis, Conceptualization. **Zhengying Shen:** Validation, Investigation. **Beibei Zhao:** Supervision, Project administration. **Nannan Wu:** Writing – review & editing, Supervision, Software, Resources, Project administration, Funding acquisition, Conceptualization.

Acknowledgements

The authors acknowledge the support received from the Natural Science Foundation of the Shandong Province (ZR2021QE164).

Supplementary materials

Supplementary material associated with this article can be found, in the online version, at doi:10.1016/j.chphma.2024.01.002.

References

[1] F. Zhang, Z. Jia, J. Zhou, J.K. Liu, G.L. Wu, P.F. Yi, Metal-organic framework-derived carbon nanotubes for broadband electromagnetic wave absorption, Chem. Eng. J. 450 (2022) 138205, doi:10.1016/j.cej.2022.138205.
[2] I. Abdall, J.Y. Cai, W. Lu, J.Y. Yu, Z.L. Li, B. Ding, Recent progress on electromagnetic wave absorption materials enabled by electrospun carbon nanofibers, Carbon 213 (2023) 118300, doi:10.1016/j.carbon.2023.11830.
[3] L.Y. Yang, L.H. Yin, C.Q. Hong, S. Dong, C. Liu, X.H. Zhang, Strong and thermostable hydrothermal carbon coated 3D needled carbon fiber reinforced silicon-boron carbonitride composites with broadband and tunable high-performance microwave absorption, J. Colloid Interface Sci. 582 (2021) 270–282, doi:10.1016/j.jcis.2020.08.030.
[4] H.S. Liang, H. Xing, Z.H. Ma, H.J. Wu, Tailoring high-electroconductivity carbon cloth coated by nickel cobaltate/nickel oxide: A transition from microwave shielding to absorption, Carbon 183 (2021) 138–149, doi:10.1016/j.carbon.2021.07.002.
[5] T.Y. Chen, S. Jiang, L.L. Li, K. Qian, J. Sun, W.W. Guo, X.D. Cai, K.J. Yu, Vertically aligned MnO_2 nanostructures on carbon fibers with tunable electromagnetic wave absorption performance, Appl. Surf. Sci. 589 (2022) 152858, doi:10.1016/j.apsusc.2022.152858.
[6] X.J. Zeng, C. Zhao, Y.C. Yin, T.L. Nie, N.H. Xie, R.H. Yu, G.D. Stucky, Construction of $NiCo_2O_4$ nanosheets-covered $Ti_3C_2T_x$ MXene heterostructure for remarkable electromagnetic microwave absorption, Carbon 193 (2022) 26–34, doi:10.1016/j.carbon.2022.03.029.
[7] X. Wang, T.F. Shi, C.L. Wan, P.A. Zong, Z.G. Liu, W. Huang, Co-enhanced electromagnetic shielding and thermoelectric performance in Bi_2Te_3 coated carbon clot, Carbon 213 (2023) 118298, doi:10.1016/j.carbon.2023.118298.
[8] S.K. Hou, Y. Wang, F. Gao, H. Yang, F. Jin, L. Ren, Q. Wu, H.L. Ge, Y.H. Wang, A novel approach to electromagnetic wave absorbing material design: Utilizing nano-antenna arrays for efficient electromagnetic wave capture, Chem. Eng. J. 471 (2023) 144779, doi:10.1016/j.cej.2023.144779.
[9] B. An, M. Wu, X.H. Yang, Z.M. Man, C.Y. Feng, X. Liang, Lightweight Co_3O_4/CC composites with high microwave absorption performance, Nano Mater. 13 (2023) 1903, doi:10.3390/nano13131903.
[10] P.B. Liu, C.Y. Zhu, S. Gao, C. Guan, Y. Huang, W. He, N-doped porous carbon nanoplates embedded with CoS_2 vertically anchored on carbon cloths for flexible and ultrahigh microwave absorption, Carbon 163 (2020) 348–359, doi:10.1016/j.carbon.2020.03.041.
[11] S.J. Zhang, B. Cheng, Z.G. Gao, D. Lan, Z.W. Zhao, F.C. Wei, Q.S. Zhu, X.P. Lua, G.L. Wu, Two-dimensional nanomaterials for high-efficiency electromagnetic wave absorption: An overview of recent advances and prospects, J. Alloys Compd. 893 (2022) 162343, doi:10.1016/j.jallcom.2021.162343.
[12] Z.H. Zhao, K.C. Kou, L.M. Zhang, H.J. Wu, High efficiency electromagnetic wave absorber derived from transition metal layered double hydroxides, J. Colloid Interface Sci. 579 (2020) 733–740, doi:10.1016/j.jcis.2020.06.123.
[13] T.Y. Chen, S. Jiang, L.L. Li, K. Qian, J. Sun, W.W. Guo, X.D. Cai, K.J. Yu, Vertically aligned MnO_2 nanostructures on carbon fibers with tunable electromagnetic wave absorption performance, Appl. Surf. Sci. 589 (2022) 152858, doi:10.1016/j.apsusc.2022.152858.
[14] X. Zeng, C. Zhao, T. Nie, Z.Y. Shen, R. Yu, G.D. Stucky, Construction of 0D/1D/2D MXene nanoribbons-NiCo@NC hierarchical network and their coupling effect on electromagnetic wave absorption, Mater. Today Phys. 28 (2022) 100888, doi:10.1016/j.mtphys.2022.100888.
[15] W.L. Luo, Y. Ma, T.X. Li, H.K. Thabet, C.P. Hou, M. Ibrahim, S. El-Bahy, B.B. Xu, Z.H. Guo, Overview of MXene/conducting polymer composites for supercapacitors, J. Energy Storage. 52 (2022) 105008, doi:10.1016/j.est.2022.105008.
[16] H.J. Wu, Z.H. Zhao, G. Wu, Facile synthesis of FeCo layered double oxide/raspberry-like carbon microspheres with hierarchical structure for electromagnetic wave absorption, J. Colloid Interface Sci. 566 (2020) 21–32, doi:10.1016/j.jcis.2020.01.064.
[17] Q.W. Li, K. Nan, W. Wang, H. Zheng, Y. Wang, Electrostatic self-assembly sandwich-like 2D/2D NiFe-LDH/MXene heterostructure for strong microwave absorption, J. Colloid Interface Sci. 648 (2023) 983–993, doi:10.1016/j.jcis.2023.06.061.
[18] Y. Wang, X.C. Di, J. Chen, L.N. She, H.G. Pan, B. Zhao, R.C. Che, Multi-dimensional C@NiCo-LDHs@Ni aerogel: Structural and componential engineering towards efficient microwave absorption, anti-corrosion and thermal-insulation, Carbon 191 (2022) 625–635, doi:10.1016/j.carbon.2022.02.016.
[19] S.K. Hou, Y. Wang, F. Gao, H. Yang, F. Jin, L. Ren, Q. Wu, H.L. Ge, Y.H. Wang, A novel approach to electromagnetic wave absorbing material design: Utilizing nano-antenna arrays for efficient electromagnetic wave capture, Chem. Eng. J. 471 (2023) 144779, doi:10.1016/j.cej.2023.144779.

[20] K. Le, Z. Wang, F.L. Wang, Q. Wang, Q. Shao, V. Murugadoss, S.D. Wu, W. Liu, J.R. Liu, Q. Gao, Z.H. Guo, Sandwich-like NiCo layered double hydroxide/reduced graphene oxide nanocomposite cathodes for high energy density asymmetric supercapacitors, Dalton Trans. 48 (2019) 5193–5202, doi:10.1039/C9DT00615J.
[21] Z. Lu, Y. Wang, X.C. Di, N. Wang, R.R. Cheng, L.Q. Yang, Heterostructure design of carbon fiber@graphene@layered double hydroxides synergistic microstructure for lightweight and flexible microwave absorption, Carbon 197 (2022) 466–475, doi:10.1016/j.carbon.2022.06.075.
[22] Y.M. Jeonga, I. Sonb, S.H. Baek, Binder–free of NiCo–layered double hydroxides on Ni–coated textile for wearable and flexible supercapacitors, Appl. Surf. Sci. 467 (2019) 963–967, doi:10.1016/j.apsusc.2018.10.252.
[23] H.J. Wu, M. Qin, L.M. Zhang, $NiCo_2O_4$ constructed by different dimensions of building blocks with superior electromagnetic wave absorption performance, Compos. B Eng. 182 (2020) 107620, doi:10.1016/j.compositesb.2019.107620.
[24] X.Q. Cai, X.P. Shen, L.B. Ma, Z.Y. Ji, C. Xu, A. Yuan, Solvothermal synthesis of NiCo-layered double hydroxide nanosheets decorated on RGO sheets for high performance supercapacitor, Chem. Eng. J. 268 (2015) 251–259, doi:10.1016/j.cej.2015.01.072.
[25] X.R. Gao, Z.R. Jia, B.B. Wang, X.M. Wu, T. Sun, X.H. Liu, Q.G. Chi, G.L. Wu, Synthesis of NiCo-LDH/MXene hybrids with abundant heterojunction surfaces as a lightweight electromagnetic wave absorber, Chem. Eng. J. 419 (2021) 130019, doi:10.1016/j.cej.2021.130019.
[26] F.Y. Gan, Q.R. Yao, J.Q. Deng, F. Wang, L.C. Cheng, Y.C. Chen, H.Y. Zhou, Y. Zhong, H.B. Yang, Y.Z. Zhao, Layered double hydroxides derived 3D flower-like FeNi@C microspheres as lightweight and high-efficient electromagnetic wave absorber, Carbon 196 (2022) 639–648, doi:10.1016/j.carbon.2022.05.037.
[27] X.Y. Shen, K. Ran, B.X. Zheng, F.Z. Chen, MOF structure engineering to synthesize accordion-like nitrogen doped carbon for enhanced microwave absorption, Mat. Lett. 321 (2022) 132373, doi:10.1016/j.matlet.2022.132373.
[28] J.W. Wang, Z.R. Jia, X.H. Liu, J.L. Dou, B.H. Xu, B.B. Wang, G.L. Wu, Construction of 1D heterostructure NiCo@C/ZnO nanorod with enhanced microwave absorption, Nano-Micro Lett. 13 (2021) 175, doi:10.1007/s40820-021-00704-5.
[29] X.J. Zeng, Y. Ning, H.H. Guo, N.H. Xie, R.H. Yu, Dual template induced assembly of 2D nanosheets to 3D porous Mo_2C/NiFe-NC networkers for electromagnetic wave absorption, Mater. Today Phys. 34 (2023) 101077, doi:10.1016/j.mtphys.2023.101077.
[30] J.W. We, X.X. Li, G. Chen, Z.N. Wang, X.J. Zhou, H.J. Wu, Controllable adjustment of cavity of core-shelled Co_3O_4@$NiCo_2O_4$ composites via facile etching and deposition for electromagnetic wave absorption, J. Colloid Interf. Sci. 594 (2021) 424–434, doi:10.1016/j.jcis.2021.03.056.
[31] X. Zhang, J. Qiao, Y.Y. Jiang, F.L. Wang, X.L. Tian, Z. Wang, L.L. Wu, W. Liu, J.R. Liu, Carbon-based MOF derivatives: Emerging efficient electromagnetic wave absorption agents, Nano-Micro Lett. 13 (2021) 135, doi:10.1007/s40820-021-00658-8.
[32] Y. Shu, T.K. Zhao, X.H. Li, L. Yang, S.Q. Cao, A. Ahmad, T. Jiang, H.J. Luo, Z.M. Jing, N.U. Ain, Flower-like Co@CoO nanohybrids assembled by crisp-rice-like quadrate flakes as high-performance electromagnetic wave absorber, Appl. Surf. Sci. 597 (2022) 153754, doi:10.1016/j.apsusc.2022.153754.
[33] J.Q. Tao, J.T. Zhou, Z.J. Yao, Z.B. Jiao, B. Wei, R.Y. Tan, Z. Li, Multi-shell hollow porous carbon nanoparticles with excellent microwave absorption properties, Carbon 172 (2021) 542–555, doi:10.1016/j.carbon.2020.10.062.
[34] Z. Xiang, C. Huang, Y.M. Song, B.W. Deng, X. Zhang, X.J. Zhu, D. Batalu, O. Tutunaru, W. Lu, Rational construction of hierarchical accordion-like Ni@porous carbon nanocomposites derived from metal-organic frameworks with enhanced microwave absorption, Carbon 167 (2020) 364–377, doi:10.1016/j.carbon.2020.06.015.
[35] A. Sheng, Y.Q. Yang, D.X. Yan, K. Dai, H.J. Duan, G.Z. Zhao, Y.Q. Liu, Z.M. Li, Self-assembled reduced graphene oxide/nickel nanofibers with hierarchical core-shell structure for enhanced electromagnetic wave absorption, Carbon 167 (2020) 530–540, doi:10.1016/j.carbon.2020.05.107.
[36] L. Chai, Y.Q. Wang, Z.R. Jia, Z.X. Liu, S.Y. Zhou, Q.C. He, H.Y. Du, G.L. Wu, Tunable defects and interfaces of hierarchical dandelion-like $NiCo_2O_4$ via Ostwald ripening process for high-efficiency electromagnetic wave absorption, Chem. Eng. J. 429 (2022) 132547, doi:10.1016/j.cej.2021.132547.
[37] J. Xu, W.J. Ma, P. He, Y.K. Zhou, X.Y. Liu, Y. Chen, P.Y. Zuo, Q.X. Zhuang, A water-induced self-assembly approach to 3D hierarchical magnetic MXene networks for enhanced microwave absorption, J. Mater. Chem. 11 (2023) 330–340, doi:10.1039/D2TA07718C.
[38] S.C. Hui, L.M. Zhang, H.J. Wu, Cationic doping induced sulfur vacancy formation in polyionic sulfide for enhanced electromagnetic wave absorption, J. Colloid Interf. Sci. 629 (2023) 147–155, doi:10.1016/j.jcis.2022.09.078.
[39] Z.H. Zhao, K.C. Kou, H.J. Wu, 2-Methylimidazole-mediated hierarchical Co_3O_4/N-doped carbon/short-carbon-fiber composite as high-performance electromagnetic wave absorber, J. Colloid Interf. Sci. 574 (2020) 1–10, doi:10.1016/j.jcis.2020.04.037.
[40] H.S. Liang, L.M. Zhang, H.J. Wu, Exploration of twin-modified grain boundary engineering in metallic copper predominated electromagnetic wave absorber, Small 18 (2022) 2203620, doi:10.1002/small. 202203620.
[41] H.S. Liang, G. Chen, D. Liu, Z.J. Li, S.C. Hui, J.J. Yun, L.M. Zhang, H.J. Wu, Exploring the Ni 3D Orbital unpaired electrons induced polarization loss based on Ni single-atoms model absorber, Adv. Funct. Mater. 33 (2023) 2212604, doi:10.1002/adfm.202212604.
[42] J.Q. Tao, L.L. Xu, C.B. Pei, Y.S. Gu, Y.R. He, X.F. Zhang, X.W. Tao, J.T. Zhou, Z.J. Yao, S.F. Tao, H.J. Wu, Catfish effect induced by anion sequential doping for microwave absorption, Adv. Funct. Mater. 33 (2023) 2211996, doi:10.1002/adfm.202211996.
[43] G. Chen, H.S. Liang, J.J. Yun, L.M. Zhang, H.J. Wu, J.Y. Wang, Ultrasonic field induces better crystallinity and abundant defects at grain boundaries to develop CuS electromagnetic wave absorber, Adv. Mater. 35 (2023) 2305586, doi:10.1002/adma.202305586.
[44] X.F. Zhou, Z.R. Jia, A. Feng, K.K. Wang, X.H. Liu, L. Chen, H.J. Cao, G.L. Wang, Dependency of tunable electromagnetic wave absorption performance on morphology-controlled 3D porous carbon fabricated by biomass, Composites Commun. 21 (2020) 100404, doi:10.1016/j.coco.2020.100404.
[45] X.L. Li, X.W. Yin, C.Q. Song, M.K. Han, H.L. Xu, W.Y. Duan, L.F. Cheng, L.T. Zhang, Self-assembly core-shell graphene-bridged hollow MXenes spheres 3D foam with ultrahigh specific EM absorption performance, Adv. Funct. Mater. 28 (2018) 1803938, doi:10.1002/adfm.201803938.
[46] F. Pan, Z.C. Liu, B.W. Deng, Y.Y. Dong, X.J. Zhu, C. Huang, W. Lu, Lotus leaf-derived gradient hierarchical porous C/MoS_2 morphology genetic composites with wideband and tunable electromagnetic absorption performance, Nano-Micro Lett. 13 (2021) 43, doi:10.1007/s40820-020-00568-1.
[47] H.X. Tan, Y.X. Wang, C.J. Wang, X.D. Xu, B.W. Cui, M.F. Li, Z.H. Xu, H.T. Jiang, Y.Q. Feng, D.L. Yang, G.S. Zhuang, Carbon nanotubes/carbon nanofibers@carbon fiber construction of 3D network hierarchical structures toward multiple synergistic losses for electromagnetic wave absorption, Vacuum 219 (2024) 112722, doi:10.1016/j.vacuum.2023.112722.
[48] S.N. Zheng, Z.H. Zeng, J. Qiao, Y. Liu, J.R. Liu, Facile preparation of C/MnO/Co nanocomposite fibers for high-performance microwave absorption, Appl. Sci. Manuf. 155 (2022) 106814, doi:10.1016/j.compositesa.2022.106814.
[49] Y.X. Qian, Y. Tao, Y. Li, J.N. Hao, C.C. Xu, W. Yan, Q.H. Jiang, Y.B. Luo, J.Y. Yang, High-performance epoxy resin with efficient electromagnetic wave absorption and heat dissipation properties for electron packaging by modification of 3D MDCF@hBN, Chem. Eng. J. 441 (2022) 136033, doi:10.1016/j.cej.2022.136033.
[50] T.Q. Hou, B.B. Wang, M.L. Ma, A.L. Feng, Z.Y. Huang, Y. Zhang, Z.R. Jia, G.X. Tan, H.J. Cao, G.L. Wu, Preparation of two-dimensional titanium carbide ($Ti_3C_2T_x$) and $NiCo_2O_4$ composites to achieve excellent microwave absorption properties, Compos. B Eng. 180 (2020) 107577, doi:10.1016/j.compositesb.2019.107577.
[51] P.B. Liu, S. Gao, Y. Wang, Y. Huang, W.J. He, W.H. Huang, J.H. Luo, Carbon nanocages with N-doped carbon inner shell and Co/N-doped carbon outer shell as electromagnetic wave absorption materials, Chem. Eng. J. 381 (2020) 122653, doi:10.1016/j.cej.2019.122653.
[52] G.X. Ding, C.F. Sun, J. Liu, Y.X. Hu, Diaminodiphenyl methane functionalized reduced graphene oxide/CoFe layered double hydroxide obtained by in situ hydrothermal as a high performance absorber, J. Solid State Chem. 322 (2023) 123949, doi:10.1016/j.jssc.2023.123949.
[53] J.W. Ding, K. Song, C.C. Gong, C.X. Wang, Y. Guo, C.S. Shi, F. He, Design of conical hollow ZnS arrays vertically grown on carbon fibers for lightweight and broadband flexible absorbers, J. Colloid Interface Sci. 607 (2022) 1287–1299, doi:10.1016/j.jcis.2021.08.189.
[54] X.J. Zeng, Y. Ning, H.H. Guo, N.H. Xie, R.H. Yu, Dual template induced assembly of 2D nanosheets to 3D porous Mo_2C/NiFe-NC networkers for electromagnetic wave absorption, Mater. Today Phys. 34 (2023) 101077, doi:10.1016/j.mtphys.2023.101077.
[55] X.F. Xu, S.H. Shi, Y.L. Tang, G.Z. Wang, M.F. Zhou, G.Q. Zhao, X.C. Zhou, S.W. Lin, F.B. Meng, Growth of NiAl-layered double hydroxide on graphene toward excellent anticorrosive microwave absorption application, Adv. Sci. 8 (2021), doi:10.1002/advs.202002658.
[56] X.Y. Zhang, C.X. Zhai, S. Zhai, R.Y. Zhang, L.L. Zhao, N.N. Huang, B.Q. Chen, The excellent microwave absorption properties of the composite structure of 3D flower-like layered double hydroxide derivatives and multi-walled carbon nanotubes, Mater. Today Chem. 33 (2023) 101708, doi:10.1016/j.mtchem.2023.101708.
[57] J. Zhou, F. Guo, J.L. Luo, G.Z. Hao, G.G. Liu, Y.B. Hu, G.P. Zhang, H. Guo, H. Zhou, W. Jiang, Designed 3D heterostructure with 0D/1D/2D hierarchy for low-frequency microwave absorption in the S-band, J. Mater. Chem. C 10 (2022) 1470–1478, doi:10.1039/D1TC04881C.